phenomenon in *L. guntea* on the aerophilic and micro-aerophilic heterotrophic gut microflora has been studied taking exclusive gill-breathing fish as control to examine the differences in terms of microbiology and gut-architecture (revealed through histology).

1. Das, B. K., Some further observation of the structure and physiology of an air-breathing loach *Lepidocepahlus* (*Lepidocephalichthys*) guntea (Ham. Buch) found in Hydrabad. In Proceeding of the 24th Indian Science Congress, Hyderabad, 1937, p. 305.
2. Mishra, K. P. and Ahamad, M. F., On the structural adaptation of an intestinal breather *Lepidocephalichthys guntea* (Ham.), a torrential loach. *Curr. Sci.*, 1986, **55**(4), 210–211.
3. Moitra, A., Sing, O. N. and Munshi, J. S. D., Microanatomy and cytochemistry of the gastro-respiretory tract of an air-breathing cobitidid fish *Lepidocephalichthys guntea*. *Jpn. J. Ichthyol.*, 1989, **36**, 227–231.
4. Singh, B. R., Yadav, A. N., Ojha, J. and Munshi, J. S. D., Gross structure and dimensions of the gills of an intestinal air breathing fish (*Lepidocephalichthys guntea*). *Copeia*, 1981, **1**, 224–229.
5. Barrow, G. I. and Feltham, R. K. A., *Manual for the Identification of Medical Bacteria*, Cambridge University Press, Great Britain, 1993, 3rd edn.
6. Cui, D., *Atlas of Histology with Functional and Clinical Correlations*, Lippincott Williams & Wilkins, Baltimore, USA, 2011.
7. Ghosh, S. K., Ghosh, B. and Chakrabarti, P., Fine anatomical structures of the intestine in relation to respiratory function of an air-breathing loach, *Lepidocephalichthys guntea* (Actinopterygii: Cypriniformes: Cobitidae). *Acta Ichthyol. Piscatoria*, 2011, **41**, 1–5.

Response of fast ice to ground penetrating radar and backscattering coefficient from scatterometer in Larsemann Hills, East Antarctica

Rajashree Vinod Bothale*, S. Anoop, Manne Gopaiah and Mehanaz Sherief

National Remote Sensing Centre, Hyderabad 500 037, India

The study presents inter-annual variations in the backscatter response of fast ice (sea ice attached to the coast) to C band Advanced Scatterometer (ASCAT) (2012–2016). It also analyses the Ground Penetrating Radar (GPR) observations collected during the 35th Indian Scientific Expedition to Antarctica (ISEA, 2015–16) for identification of different fast ice features and to measure fast ice depth in the Larsemann Hills area, East Antarctica. Apart from clear demarcation of features like melt water channels, frozen icebergs within fast ice and underlying topography near island, GPR provided fast ice depth information, which was used to understand backscatter response. The seasonal variations of C band backscatter were caused due to changes in snow thickness, time of freezing and sporadic melt/freeze events apart from summer melt. The backscatter response to NOAA high resolution blended daily sea surface temperature (SST) variations indicate that sudden rise/fall in backscatter during winter is probably due to sporadic melt/freeze events caused by rise/fall in SST. The results show volumetric contribution from sheet ice and domination of snow metamorphism towards increase in backscatter over fast ice. This study highlights the importance of monitoring backscatter response of fast ice to determine its state and condition. Depending on the characteristics of backscatter inter-annual curve, information about time of freeze up, melt season, ice build-up, and sporadic freeze/thaw events can be inferred which play an important role in the energy budget of Antarctica.

Keywords: Antarctica, ASCAT, fast ice, GPR, Larsemann Hills.

THE Larsemann Hills area is located on the south-eastern coast of Prydz Bay, Princess Elizabeth Land, in East Antarctica. Because of its ice free area of approximately 40 sq. km, this region is environmentally, scientifically and logistically significant. The ice-free area consists of two major peninsulas (Stornes and Broknes), four minor peninsulas, and approximately 130 near-shore islands[1]. Indian research base 'Bharati' is located between Thala Fjord and Quilty bay, east of Stornes Peninsula in Antarctica at 69°24.41′S, 76°11.72′E. Fast ice formation in this area varies every year with varying ice thickness surrounding Bharati station. The fragmented land is bounded by open sea in the North and polar sheet ice in the South. Strong winds blow from NE to SW[2]. Temperature during the study period (2012–2017) reached as high as 6.23°C in summer and dipped to –36.26°C in winter. The fast ice in this area is single year ice which states disintegrating upon the arrival of supply ship to Bharati station. This leads to the development of flaws in ice, which act as zones of high backscatter.

Researchers studied the snow on Antarctic sea ice using data collected over 10 years to characterize snow thickness, snow type and their geographical and seasonal variations; snow grain size, density, and salinity; frequency of occurrence of slush; thermal conductivity, snow surface temperature, and temperature gradients within snow; and the effect of snow thickness on albedo.
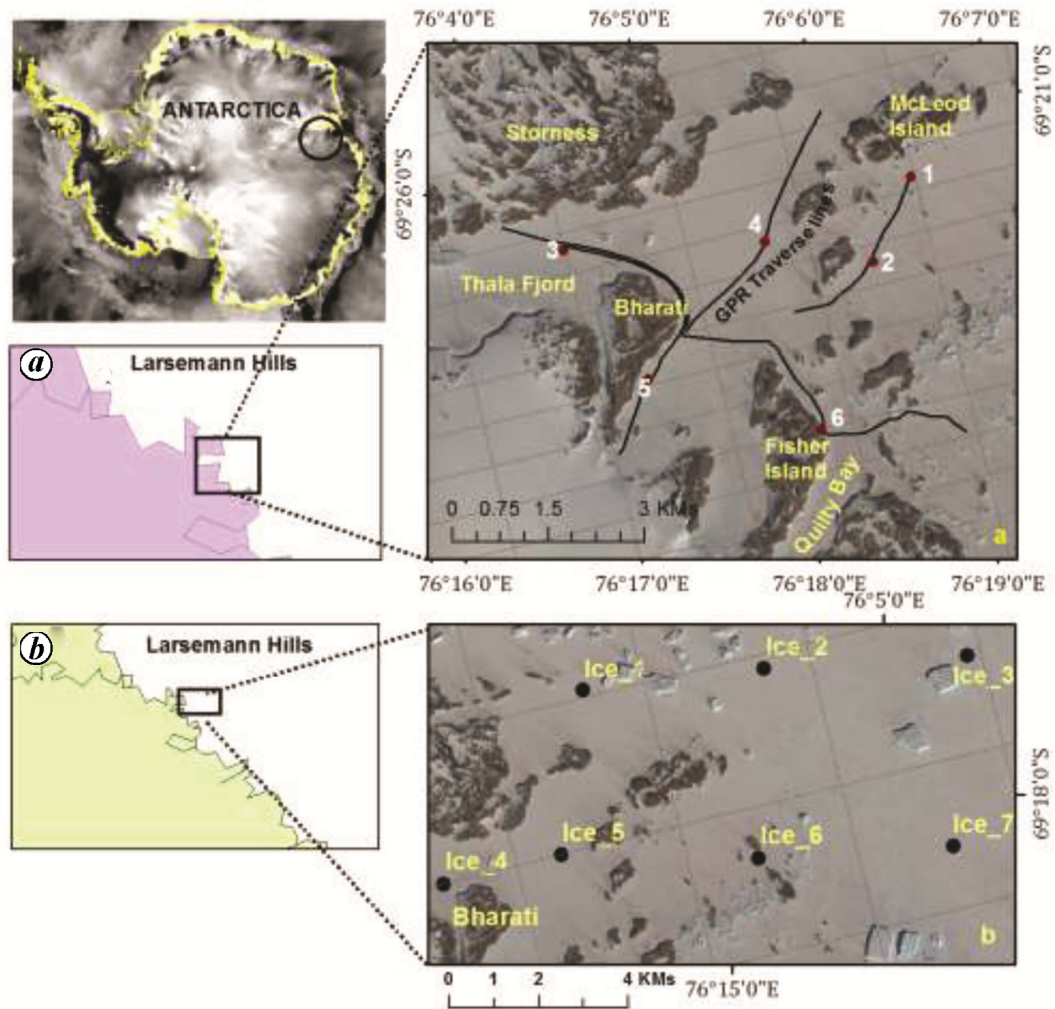
*For correspondence. (e-mail: rbothale@gmail.com)

Figure 1. Location map of sites of GPR profiling (*a*) over fast ice near Larsemann Hills area. (*b*) Observations points for detailed analysis.

They found that highly dynamic and variable weather conditions in the Antarctic sea-ice with periods of high temperatures in winter and strong winds often accompanying snowfall result in numerous snow layers with different physical characteristics[3].

Fast ice affects surface energy balance due to its high albedo, absorbed insolation and by dampening the ocean-atmosphere heat exchange[4]. Seasonal variations and undulations in fast ice properties combined with melt–freeze cycle have a large impact on the regional energy budget. A study demonstrated that a delayed freeze-up can decrease the snow pack thickness in winter through decreased snow accumulation on fast ice[5]. Microwave instruments are sensitive to dielectric properties related to the amount of liquid water content on the surface and provide valuable information over fast ice[6,7]. The single year ice goes through different phases of freezing and melting every year resulting in changes in the microwave signals.

Snow/ice characteristics in Antarctica are different from that in Arctic with varying physical characteristics.

Field investigations of Ku band radar were carried out for its penetration into snow cover on Antarctic fast ice and the snow pit studies revealed that the snow/ice surface was the dominant scattering surface for snow without morphological features or flooding. Scatterometer provides valuable information over ice/snow features[8]. Signal penetration depends on the characteristics of snow/ice. High radar backscatter regions on Antarctic fast ice were studied using QuikSCAT data and it was observed that high backscatter signals close to marginal ice zones are caused by metamorphous snow, which forms through re-freezing after short term melt events[9]. Compared to the Arctic, snow cover thickness is higher in Antarctica, often depressing the ice beneath the sea surface, thereby causing flooding at the snow–ice interface[8]. The backscatter from winter snow covered first year ice is influenced by the combination of (1) surface scattering from air–snow interface, dry snow–brine wetted snow interface and snow–sea ice interface and (2) volume scattering from the dry snow, brine wetted snow and upper layer of sea ice[10].
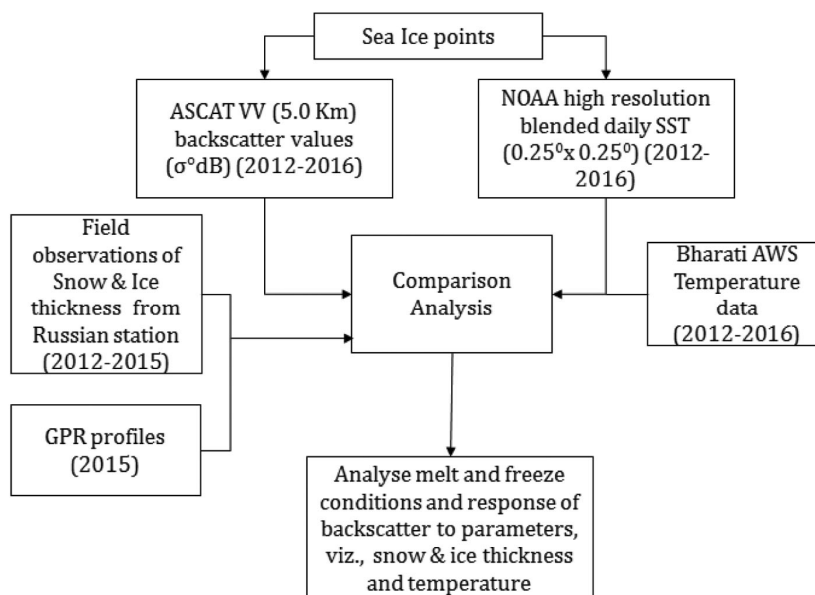
Figure 2. Flowchart for methodology.

Advanced Scatterometer (ASCAT) is an active microwave instrument mounted on three polar orbiting 'European Organization for the Exploitation of Meteorological Satellites (EUMETSAT)/European Space Agency (ESA)' satellites[11], which currently provides daily data over Antarctica using C Band (5.26 GHz, 5.7 cm wavelength, VV polarization) scatterometer. During 2011–2016 analysis of ASCAT and Oceansat Scatterometer (OSCAT) data over sheet ice revealed different behaviours over the accumulation zone[12]. Ground penetrating radar (GPR) is a high resolution geophysical technique, which provides ground information using different frequency band antenna. Physical measurements of fast ice depth are expensive in terms of cost and efforts and sometimes not possible during the beginning of austral summer. Data obtained from GPR over fast ice help in understanding ice characteristics and its response to scatterometer. Studies were carried out on the Quilty Bay area using 200 MHz antenna which recorded variations in fast ice thickness during austral winters of 2010–2014 (ref. 2). High resolution GPR profiles were studied over lake ice in McMurdo Dry Valleys, Antarctica using 850 MHz GPR (ref. 13).

A small area of Antarctic fast ice is studied (Figure 1) through satellite scatterometer observations, ground based GPR observations and collected field observations by Russian Progress II station. This was used to characterize fast ice and study spatial and seasonal variations in its backscatter response.

Observations were taken on fast ice near Bharati Indian station using GPR. This study attempts to present qualitative and quantitative assessment of fast ice using GPR which was used to understand the seasonal variations in

its backscatter response through satellite based scatterometer observations. The GPR and scatterometer observations are correlated with field observations obtained from Russian station, Progress II in Antarctica.

GPR profiles were acquired for different fast ice features, the data were processed and analysed together with analysis of VV polarized daily ASCAT data (downloaded from website of Brigham Young University) at 5 km grid size for the period 2012–2016 to understand the variation in backscatter over fast ice (Figure 2). Daily temperature data collected from Bharati station was also analysed and correlated with fast ice conditions. NOAA high-resolution blended sea surface temperature (SST) data from Earth System Research Laboratory (ESRL)[14,15] website was downloaded at 0.25° lat × 0.25° long grid[16] and analysed. The entire study area was covered in one grid element of SST data. Fast ice and snow depth data collected by Russian station Progress II was also used.

Over the sites shown in Figure 1 near Bharati Indian station, Antarctica, GPR surveys were carried out using Geoscanners AB, Akula 9000 GPR from Sweden at 400 MHz and 200 MHz frequency during December 2015–January 2016 (summer season in Antarctica). A Garmin GPS was used to locate the position of observations. To collect observations over fast ice, the GPR was tied behind a sledge, which was attached behind skidoo (Figure 3). The skidoo moved at a slow speed to enable observations using GPR. Figure 3 also shows the field photograph of icebergs and general sea ice condition along with snow grains and hole in the snow on sea ice.

GPR data was acquired in ice mode and dielectric constant was kept at 1.14. Survey parameters like frequency, scan, range etc., were set after doing few trial runs before

Figure 3. GPR observations over fast ice (*a*) with GPR tied up to Skidoo (*b*) field photo of sea ice with icebergs and (*c*) snow structure.
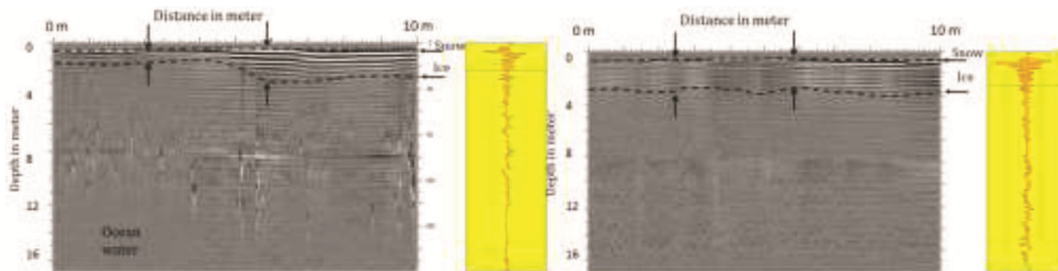

Figure 4. GPR profiles en route McLeod island from Bharati station (points 1 and 2 in Figure 1 *a*).

the actual survey. The survey done using 200 MHz and 400 MHz were compared for one run. The 200 MHz antenna was used for subsequent observations to achieve higher penetration. Range used in the analysis was 200 ns with sample/scan value as 800 and scan/m as 44. Surface removal, DC removal, dewow, filtering, background removal and filtering functions were performed for processing of GPR data.

GPR observations over fast ice near Bharati Indian station provide qualitative and quantitative information about thickness of fast ice, on a real time basis. Analysis reveals that fast-ice thickness varies over the ocean surface and around 2 m of ice thickness is the characteristic of single year ice. On the route near McLeod Island (Figure 1 *a* points 1 and 2), snow thickness of 0.4 m to 0.6 m was observed over varying ice thickness of 0.8 m to 2 m (Figure 4). The ship route was characterized by average snow thickness of 0.3 m to 0.4 m over maximum of 2 m fast ice.

In continuation of the observations taken by Russian Antarctic station Progress II on 28 August and 29 November 2015, observations taken during the 35th expedition on 4 December (Figure 1 *a* point 3) showed a slight reduction in snow thickness over similar ice thickness near Stornes (Figure 5). Many melt water channels were observed on the fast ice GPR profiles on the ship route (Figure 1a point 4 and Figure 6). Presence of frozen icebergs can be seen on the profile (Figure 6) and bottom topography near the Bharati and Fisher (Figure 1 *a* points 5 and 6) islands is also visible on profiles taken parallel

to these islands (Figure 7). It is indicative of the continuity of topography[2]. Below the 0.3 m snow surface, a 1 to 1.2 m ice layer is seen above the bottom rock layer (around 4 m thickness). Based on GPR observations, an interpolated fast ice depth layer was generated, which shows lesser development of fast ice in Thala Fjord lying between Bharati island (North Grovnes) and Stornes peninsula. These results are similar to the results shown in another study[2], indicating a pattern in development of fast ice in the study area. Maximum ice thickness was observed between Stornes and McLeod Island.

ASCAT VV polarization data was studied between 2012 and 2016 to know the backscatter response of fast ice. With ASCAT's 5 km resolution, pixels dominant in sheet ice (Figure 1 *b*, Point Ice_4) show response similar to sheet ice where volumetric component dominates the backscatter response. The backscatter values of such pixels are high without much fluctuation, whereas pixels over fast ice show large fluctuation due to continuous melt/freeze cycles resulting in changes in dielectric constant (Figure 8). The 'points near' corresponds to average backscatter of Ice_1 and Ice_5 (Figure 1 *b*) and 'points away' corresponds to average backscatter of Ice_3 and Ice_7. Various studies also indicate that volume echo dominates the backscatter over sheet ice[17,18].

The fast ice in this region is single year ice and does not survive in summer. Changing sea/ice conditions and melt/freeze cycles cause variations observed in backscatter response over fast ice. A large portion of the first year ice has its origin as pancake and frazil ice. Because of
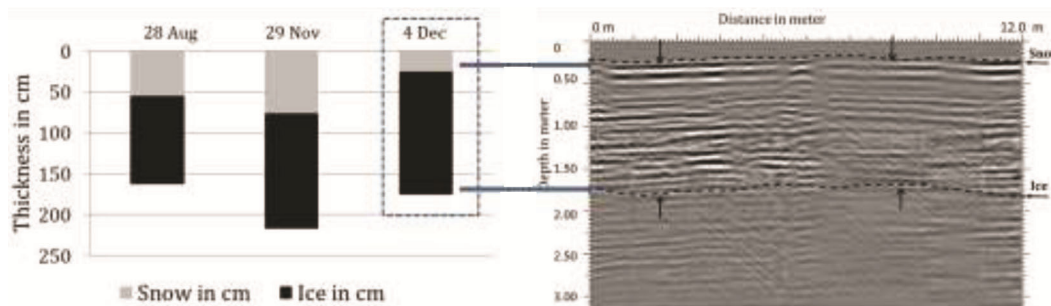
Figure 5. Comparison of field and GPR based observations near Stornes island (Point 3 in Figure 1 *a*).
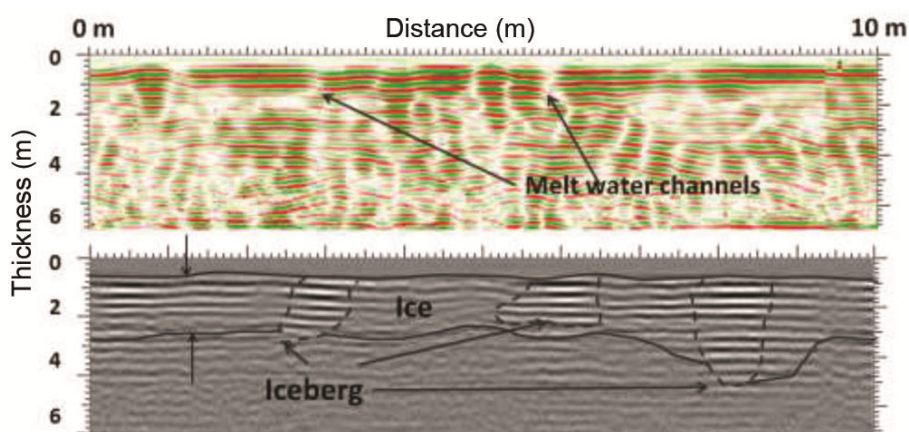

Figure 6. Reflective pattern of different fast ice features (point 4 in Figure 1 *a*).
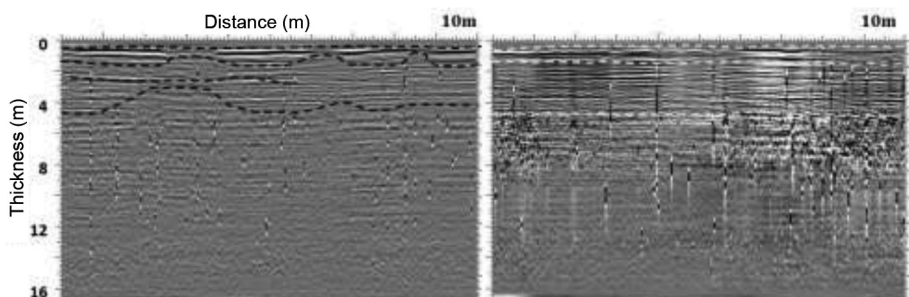

Figure 7. Sub surface profile parallel to Bharati island and Fisher island (points 5 and 6 in Figure 1 *a*).

heavy snow load, snow–ice interface is frequently flooded causing an increase in backscatter levels. Mixing of flooded floes with unflooded floes generates a diverse range of signatures in this region. Changes in backscatter begin with the freezing of open water and the seasonal variations are caused due to change in physical properties, dielectric constant, surface roughness of ice and snow layers (Figure 9). Figure 9 also shows the plot of daily average, backscatter calculated from ASCAT data. The graph starts from freezing of open water and continues till the end of the year. A reduction in backscatter is observed, due to the formation of new smooth ice. With the reduction of dielectric constant and the scale of sur-face roughness, backscatter from new ice reduces. The signal strength depends upon prevailing environmental conditions. In case of high winds, increased roughness will raise the backscatter. The lowest point of the curve in March indicates complete formation of new smooth ice. The rise in backscatter during March–April is due to the formation of frost flowers, that increase surface roughness. With further reduction in temperature and cold air, frost flowers continue to develop, change the grain size and cause further rise in backscatter. This increase continues till the full development of frost flowers after which reduction in backscatter is observed due to snowpack infiltration and accumulation. A layer of accumulating

snow of increasing depth overlying a scattering layer created by the melt metamorphosis of snow and firn layers decreases the backscatter measurements over time, resulting in decreasing winter season backscatter signatures[17]. The fall, rise and fall sequence of backscatter during July and September is probably due to refreezing after snow melt events caused by sporadic rise in SST (Figure 10). The sporadic events were probably caused by entry of warm air during 2013 and 2014, that initiated melt. The water refreezes again with drop in temperature, but not before causing changes in the micro structure of the snow. The ice grains become round in the melting process and join during refreezing process. The new grain size formed is responsible for sudden increase in the backscatter. The approaching extra tropical cyclone causes occasional rise in air temperature above 0°C causing short duration melt[9]. SST is a key for formation of sea ice and sea ice condition. Air temperature and SST increase during approaching summer and melt surface snow as

Figure 8. Backscatter response over sheet ice and pixel near and far from coast.

Figure 9. Seasonal and temporal variations in backscatter from fast ice.

observed during the months of November–December. With further rise in air temperature, snow surface layers experience water that absorbs C band microwaves and reduces the penetration depth which causes a sudden drop in backscatter indicative of melt events. During austral summer when the temperature increases above 0°C, SST also shows rise in temperature (Figure 10).

The increase in snow thickness (Figure 11) can be attributed to increase in backscatter. Thick snow induces higher temperature at snow–ice interface causing increase in brine volume which acts as effective scatterer thereby increasing the radar backscatter[10]. The year-wise plots of backscatter, fast ice and snow depth (Figure 11) show the inter-annual variations caused due to prevailing climatic conditions.

The field data for fast ice thickness is generally not available during the formation of new ice, but by extending the ice thickness line in Figure 11, one can see that the rise in backscatter coincides with ice thickness of around 30–40 cm, beyond which a drop in backscatter is observed due to accumulation of snow (Figure 9).

The presence of peak and trough in the month of January indicate varying sea conditions (frozen ice and melt) in respective years. The years 2013 and 2015 observed early snow melt followed by disintegration of fast ice caused by the lead of ship. The small rise in backscatter around February is due to rough fast ice formed and due to ice disintegration. The years 2012 and 2014 had undisturbed ice even by mid February as evident from Figure 11 (high backscatter in January followed by drop due to snow melt). By monitoring the microwave backscatter, it is possible to determine the state of fast ice. Depending upon the characteristics of seasonal curve, information about time of freeze up, melt season, ice build-up, and sporadic freeze/thaw events can be inferred. Melt-freeze transitions of sea-ice cover and overlaying snow have a large impact on the energy budget[4]. In fast ice areas with thick snow, surface flooding and freezing of slush at the snow–ice interface is observed which contributes to the formation of sea-ice in turn affecting the total sea-ice volume[19]. Small changes in the timing of the transitions may have a large impact on the regional energy budget. An earlier melt and delayed freeze–up can increase the heat content of the ocean. The thinner ice cover is associated with delayed freeze–up[20]. In the present study we tried to find a visual correlation between backscatter and the thickness of fast ice (Figure 11). Earlier formation of fast ice and later ending of frost flower stage, resulted in increase in fast ice thickness. The thickest fast ice was observed for the year 2014 followed by 2015. The average temperature as well as SST was lower during 2014 and 2015 (Figure 10) in comparison to other years where snow/ice was less thick (Table 1). Table 1 shows the average weather conditions and snow/ice thickness during the study period. As the backscatter response is cyclic, efforts were made to find the correlation between
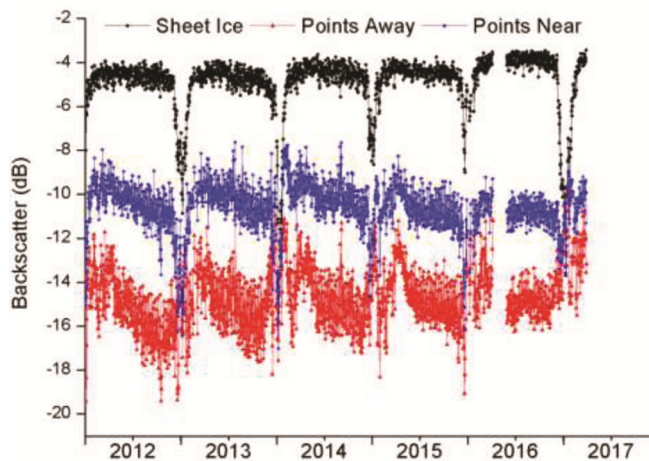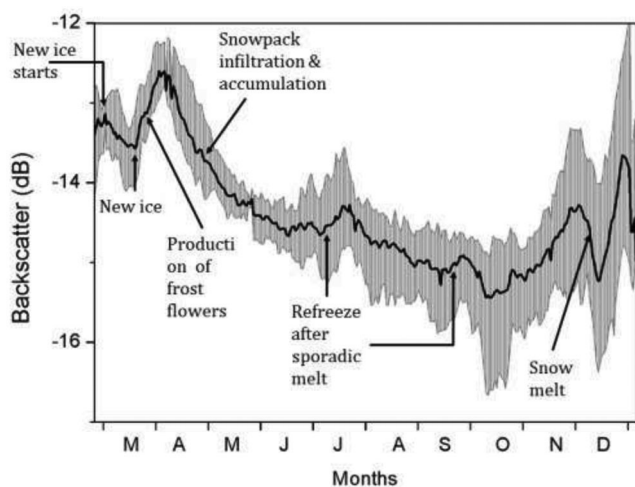
Table 1. Average weather conditions and snow/ice thickness during the study period

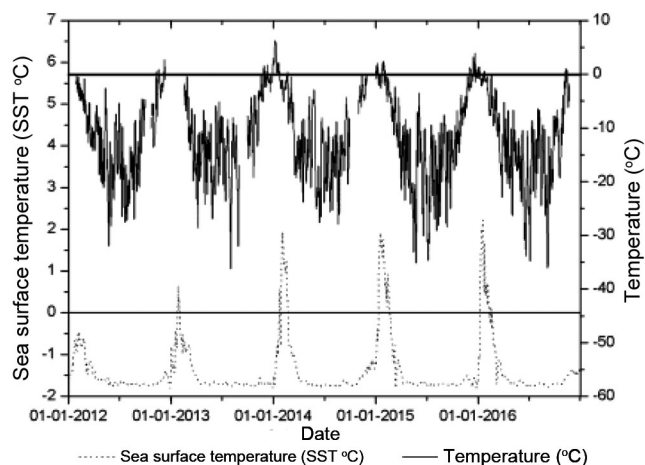| Year	Average annual temperature of Bharti station	Bharati temperature (May–November)	Average SST	Average thickness in cm during May–November (field data from Progress station, Antarctica)	
				Snow	Ice
2012	−11.72	−13.45	−1.7	25.85	89.13
2013	−11.56	−13.11	−1.69	16.53	95.20
2014	−10.99	−13.48	−1.74	32.15	114.96
2015	−11.53	−15.69	−1.71	36.05	100.96

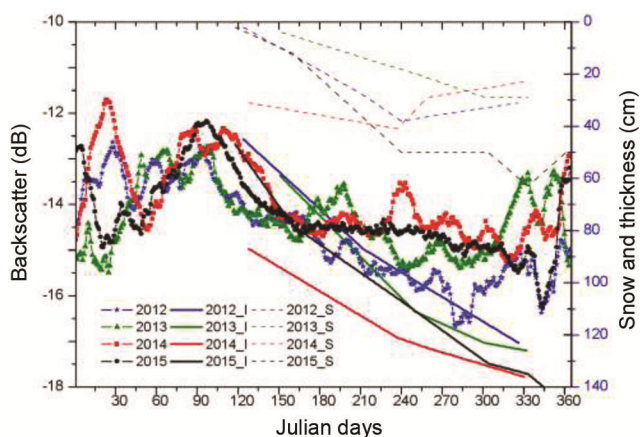**Figure 10.** Air temperature over Bharati station and SST over study area.

Figure 11. ASCAT VV polarization moving average backscatter response over different years. Line and marker symbol lines indicate VV backscatter, solid line represents ice thickness and dash lines indicate snow thickness observed in the study area.

different parameters during peak winter season. No correlation was observed between backscatter coefficient, snow/ice thickness and air temperature. The backscatter depends upon many parameters including air temperature, SST, thickness of snow and ice and summer melt/freeze.

GPR observations using 200 MHz antenna clearly demarcated fast ice features and depth over study area, and were used for inferring general fast ice condition. Features like frozen icebergs, melt water channels and the underlying topography were clearly identified. The measured fast ice depth was in continuation to the observed ice depth by Russian station Progress II. The seasonal variations of C band backscatter indicated that the changes in backscatter were caused due to increased/decreased snow thickness, early/late onset of freeze and sporadic melt/freeze events apart from summer melt. Sporadic melt/freeze events are responsible for changes in backscatter response and thickness. The backscatter curve can infer information about initiation of summer melt, melt season, ice buildup, fall freeze-up, etc. which are important parameters in building of fast ice. With continuous monitoring of backscatter, it may be possible to determine the physical state of fast ice. More ground truth information is needed for quantitative analysis of backscatter and sea/snow depth over fast ice.

1. ATCM XXXVII final report, 2014, Larsemann Hills, East Antarctica Antarctic Specially Managed Area Management Plan. Measure 15, Annex.
2. Shah, M. Y., Ayemi, K. K. and Shrivastava, P. K., GPR survey and physical measurements of sea ice in quilty Bay, Larsemann Hills, East Antarctica and its correlation with local atmospheric parameters. *J. Geol. Soc. India*, 2017, **90**, 371–377.
3. Massom *et al.*, Snow on Antarctic fast ice. *Rev. Geophys.*, 2001, **39**(3), 413–445.
4. Mortin, J., Howell, S., Wang, L., Derksen, C., Svensson, G., Graversen, R. and Schroder, T. M., Extending the QuikSCAT record of seasonal melt–freeze transitions over Arctic sea ice using ASCAT. *Remote Sensing Environ.*, 2014, **141**, 214–230.
5. Hezel, P. J., Zhang, X., Bitz, C. M., Kelly, B. P. and Massonnet, F., Projected decline in spring snow depth on Arctic sea ice caused by progressively later autumn open ocean freeze-up this century. *Geophys. Res. Lett.*, 2012, **39**(17), L17505.\
6. Bothale, Rajashree V., Rao, P. V. N., Dutt, C. B. S., Dadhwal, V. K. and Maurya, D., Spatio-temporal dynamics of surface melting over Antarctica using OSCAT and QuikSCAT scatterometer data (2001–2014). *Curr. Sci.*, 2015, **109**(4), 733–744.
7. Oza, S. R., Spatial-temporal patterns of surface melting observed over Antarctic ice shelves using scatterometer data. *Antarct. Sci.*, 2015, **27**(4), 403–410.
8. Willat, R. C., Giles, K. A., Laxon, S. W., Stone-Drake, L. and Worby, A. P., Field Investigations of Ku-Band radar penetration into snow cover on Antarctic Sea Ice. *IEEE Trans. Geosci. Remote Sensing*, 2010, **48**(1), 365–372.
9. Willmes, S., Haas, C. and Nicolaus, M., High radar-backscatter regions on Antarctic sea-ice and their relation to sea-ice and snow

properties and meteorological conditions. *Int. J. Remote Sensing*, 2011, **32**(14), 3967–3984.

10. Gill, J. P. S., Yackel, J. J., Gekdsetzer, T. and Fuller, C., Sensitivity of C-band synthetic aperture radar polarimetric parameters to snow thickness over landfast smooth first year sdea ice. *Remote Sensing Environ.*, 2015, **166**, 34–49.

11. Vogelzang, J. and Stoffelen, A., Scatterometer wind vector products for application in meteorology and oceanography. *J. Sea Res.*, 2012, **74**, 16–25.

12. Bothale, Rajashree, Anoop, S., Rao, V. V., Dadhwal, V. K. and Krishnamurthy, Y. V. N., Understanding relationship between melt/freeze conditions derived from spaceborne scatterometer and field observations at Larsemann hills, East Antarctica during austral summer 2015–16. *Curr. Sci.*, 2017, **113**(4), 733–742.

13. Dugan, H. A., Arcone, S. A., Obryk, M. K. and Doran, P. T., High-resolution ground-penetrating radar profiles of perennial lake ice in the McMurdo Dry Valleys, Antarctica: Horizon attributes, unconformities, and subbottom penetration. *Geophysics*, **81**(1), WA13-WA20.

14. https://www.esrl.noaa.gov/psd/data/gridded/

15. https://www.esrl.noaa.gov/psd/data/gridded/tables/sst.html

16. Reynolds, R. W., Smith, T. M., Liu, C., Chelton, D.B., Casey, K. S. and Schlax, M. G., Daily high resolution blended analyses for sea surface temperature. *J. Climate*, **20**, 5473–5496.

17. Tedesco, M., *Remote Sensing of the Cryosphere* (ed. Tedesco, M.), Library of Congress Cataloging-in-Publication Data, Wiley Blackwell, 2015.

18. Adodo, F. I., Remy, F. and Picard, G., Seasonal variations of the backscattering coefficient measured by radar altimeters over the Antarctic Ice Sheet. *Cryosphere*, 2018, **12**, 1767–1778.

19. Markus, T. and Cavalieri, D. J., Interannual and regional variability of Southern Ocean snow on sea ice. *Ann. Glaciol.*, 2006, **44**, 53–57.

20. Dumas, J. A., Flato, G. M. and Brown, R. D., Future projections of land fast ice thickness and duration in the Canadian Arctic. *J. Climate*, 2006, **19**(20), 5175–5189.

A damage constitutive model for the intermittent cracked rock mass under the planar complicated stress condition

Hongyan Liu* and Fengjin Zhu

College of Engineering and Technology,
China University of Geosciences (Beijing), Beijing 100083, P.R. China

The calculation of rock mass damage induced by the intermittent crack is the premise for establishment of the rock mass damage constitutive model (DCM). However, there are two shortcomings in the previous calculation methods of the rock mass damage: (a) it only considers the crack geometry or strength parameters, and does not consider its deformation parameter such as normal and shear stiffness; and (b) the influence of loading condition of the rock mass is not considered. This study focuses on intermittent cracked rock mass under the planar complicated stress condition and calculates its damage tensor. The proposed calculation method of rock mass damage considers the crack parameter such as length, dip angle, internal friction angle, normal and shear stiffness (internal factor) as well as the loading condition (external factor). The corresponding DCM for the intermittent cracked rock mass is then set up. The calculation examples validate that the proposed model can reflect the influence of crack parameter and loading condition on the rock mass mechanical behaviour.

Keywords: Damage, intermittent cracked rock mass, planar complicated stress condition, stress intensity factor, strain energy density criterion.

THE mechanical behaviour of rock mass such as its strength and deformability under the complicated stress condition is one of the most important issues in practical engineering. Cracks affect the rock mass mechanical behaviour and failure mode to a large extent[1–6]. Wang and Huang[1,2] set up a constitutive model for the rock mass to reflect its strength and deformation anisotropy caused by the persistent joint. Tokiwa *et al.*[3] found that the rock mass deformability was controlled by the fault system in a shaft excavation in soft rock. Sari[4] assumed that the rock mass mechanical property was affected by the discontinuity characteristic and intact rock property. Through experimental and numerical analysis, Sagong *et al.*[5] found that the joint dip angle had much effect on the rock fracture and joint sliding behaviours around an opening in a jointed rock mass. Khani *et al.*[6] found that the rock mass deformational modulus and Poisson's ratio greatly decreased with the increase in fracture intensity. As the cracks are often many and intermittent, their influence on rock mass mechanical property cannot be

*For correspondence. (e-mail: lhy1204@cugb.edu.cn)